agents. A functional analysis of these genes was performed using EASE, and the results are listed in Table 1. The results showed that genes associated with cell-cycle regulation, mitosis or apoptosis were significantly upregulated by the antimicrotubules agents. Among the downregulated genes, 141 genes that were associated with cell communication and morphogenesis were selected. These results suggested that transcription regulation by antimicrotubule agents results in the biological inhibition of microtubule dynamics.

Drug characterization using molecular reference profiles

Focusing on the 'reference profiles' of the drug-induced genomic response, we compared the profiles of TZT-1027 with those of five conventional antimicrotubule agents and the mother compound, D10.

A principle component representation of the whole gene set in three-dimensional space clearly showed the relationship between TZT-1027 and the other six reference profiles (Figure 1). All the drugs were separated according to each drug class in this profile. In comparison with these reference profiles, TZT-1027's profile was similar to that of D10 but different from those of the taxanes and *Vinca* alkaloids.

To investigate the differences in genomic response between the drug classes, we selected discriminatory genes that were regulated differently between the drug classes, compared with the complete gene set. Table 2 shows the genes whose expression profiles differed after exposure to dolastatins (TZT-1027 and D10) and the other antimicrotubule agents. The most discriminatory gene in this gene set was the drug-resistant gene, *GSTO1*. Using this gene set, the classes of antimicrotubule agents could be clearly separated (Figure 2a). Discriminatory gene sets for the taxanes and *Vinca* alkaloids were obtained in a similar manner (Tables 3 and 4). The profiles of the discriminatory gene sets for the taxanes and *Vinca* alkaloids are shown in Figure 2b and c.

To further characterize TZT-1027, the genes that were regulated differently after exposure to TZT-1027 and D10 were investigated. Six genes that were regulated differently by a factor of more than one in a log ratio after exposure to each agent were selected (Table 5). Four cytoskeletal genes were included in this group. A three-dimensional representation using these six genes demonstrated that the profiles

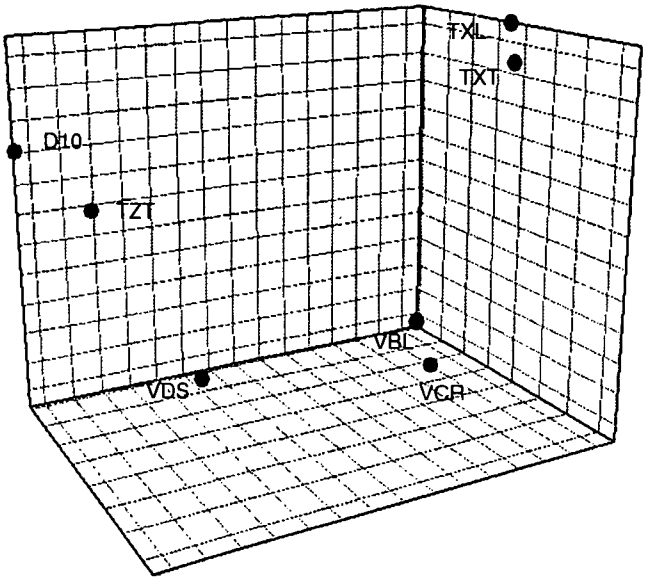

Figure 1 Three-dimensional representation of antimicrotubule agents according to a principle component analysis of the gene expression data for 588 genes. In this analysis, samples with similar expression profiles lie closer to each other than those with dissimilar profiles. The graph shows a robust class separation into three major categories: dolastatins, *Vinca* alkaloids and taxanes. TZT, TZT-1027; dolastatin 10, D10; VDS, vindesine; VCR, vincristine; VBL, vinblastine; TXL, paclitaxel; TXT, docetaxel.

Table 2 Discriminatory genes of dolastatins (D 10 and TZT-1027)

GB	*Symbol*	*Description*	*Log ratio*			
			D10	*TZT*	*VA*	*TX*
Upregulated genes						
U90313	GSTO1	Glutathione-*S*-transferase homolog	0.905	0.189	−0.818	−0.706
Z30183	TIMP3	Tissue inhibitor of metalloproteinase 3	0.703	0.481	−0.343	−0.859
U46461	DVL	Disheveled, dsh homolog 1	0.206	0.396	−0.542	−0.444
J00124	KRT1	50 kDa type I epidermal keratin	0.190	0.278	−0.643	−0.219
M57765	IL11	Interleukin 11	0.124	0.454	−0.342	−0.493
M74088	APC	Adenomatosis polyposis coli	0.040	0.069	−0.224	−0.582
Downregulated genes						
U02570	RhoGAP1	Rho-related small GTPase protein activator	−0.048	−0.076	0.433	0.248
J04177	COL11A1	Collagen, type XI, alpha 1	−0.048	−0.290	0.388	0.074
X72925	DSC1	Desmocollin-1	−0.117	−0.051	0.346	0.388
U35835	DNA-PK	DNA-dependent protein kinase	−0.215	−0.241	0.596	0.648
M65290	IL12B	Interleukin 12 beta	−0.322	−0.134	0.351	1.070

Abbreviations: GB, genebank accession number; D10, dolastatin 10; TZT, TZT-1027; VA, average of *Vinca* alkaloids including vincristine, vindesine, vinblastine; TX, average of taxanes including paclitaxel and docetaxel.

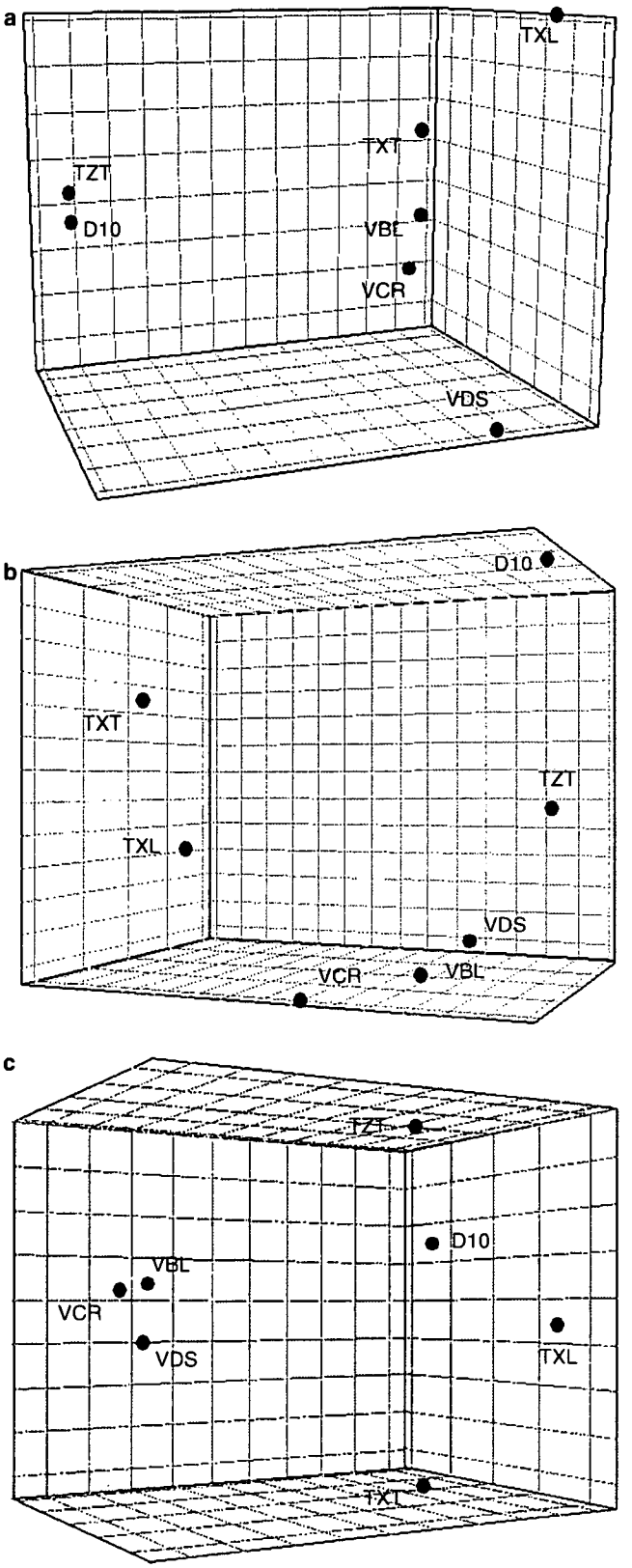

of the taxanes and *Vinca* alkaloids differed from those of TZT-1027 and D10 (Figure 3).

Validation of discriminatory genes by RT-PCR

The identified discriminatory genes GSTO1 and TIMP3 were validated using real-time RT-PCR (Figure 4). To investigate whether the genomic responses of these genes depended on the cytotoxicity levels, the RT-PCR experiment was performed at different cytotoxicity levels (IC_{90} and IC_{10}) of TZT-1027. The results are summarized in Figure 5. These findings suggested that the selected genomic responses might not depend on the cytotoxicity levels, whereas the genomic response of GSTO1 demonstrated a dose dependency.

Discussion

In the present study, we characterized the novel antimicrotubule agent TZT-1027 using a microarray analysis. Dolastatins belong to a class of microtubule-destabilizing agents, but this classification is not sufficient for clinical use. Despite similarities in their mechanism of action and structure, antimicrotubule agents differ in their antitumor and toxicologic profiles.[24] It now seems that the most important action of antimicrotubule agents is not the regulation of microtubule-polymer mass (polymerization and depolymerization), but the suppression of spindle-microtubule dynamics.[25] Furthermore, many of the drugs act not only on microtubules, but also on soluble tubulin, and the location of the specific binding site in tubulin and microtubules greatly affects the response of the microtubule system to the drug.[25] Therefore, to characterize the novel antimicrotubule agent TZT-1027, we analyzed drug-induced changes in gene expression using the microarray technique and compared the molecular profiles with those induced by the mother compound, D10, and other well-known antimicrotubule agents, such as *Vinca* alkaloids and taxanes.

For the profiles, we evaluated the IC_{50} value of each drug using a growth inhibitory assay. We aimed to categorize the drugs based on their mechanisms of action; therefore, the changes in gene expression were, of necessity, induced at the same cytotoxicity level. The resulting expression profiles were obtained using a microarray containing ~600 key genes applicable to antimicrotubule drug research, including genes involved with microtubule dynamics, cell-cycle regulation, angiogenesis and the extracellular matrix as well as cell adhesion receptors, oncogenes and tumor-suppressor genes. We focused on changes in gene expression because gene regulation should be correlated with the protein status modulated by the drugs.

Figure 2 Spatial class separation of antimicrotubule agents using specific discriminatory genes. The axes represent the first three linear discriminants of the expression levels of (**a**) 11 dolastatin-discriminatory genes from Table 2, (**b**) 9 taxane-discriminatory genes from Table 3 and (**c**) 5 *Vinca* alkaloid-discriminatory genes from Table 4. TZT, TZT-1027; dolastatin 10, D10; VDS, vindesine; VCR, vincristine; VBL, vinblastine; TXL, paclitaxel; TXT, docetaxel.

Table 3 Discriminatory genes of taxanes (paclitaxel, docetaxel)

GB	*Symbol*	*Description*	*Log ratio*			
			TX	*VA*	*D10*	*TZT*
Upregulated genes						
X02492	G1P3	Interferon-induced protein 6–16 precursor	1.122	−0.397	−1.150	−0.902
Y10256	NIK	Serine/threonine protein kinase	0.637	−0.951	−0.595	−0.287
U72661	NINJ1	Ninjurin 1	0.481	−0.154	−1.015	−0.448
M65199	ET2	Endothelin 2	0.444	−0.488	−2.185	−1.507
X54936	PlGF	Placenta growth factor	0.345	−0.235	−0.677	−0.602
X01992	IFN-gamma	Interferon, gamma	0.251	−0.929	−1.005	−1.583
Downregulated genes						
AF010309	PIG3	Tumor protein p53 inducible protein 3	−0.036	0.366	0.957	0.652
M76125	UFO	Tyrosine-protein kinase receptor UFO precursor	−0.132	0.201	0.020	0.329
U39657	MKK6	Mitogen-activated protein kinase 6	−0.204	0.554	0.740	0.368

Abbreviations: GB, genebank accession number; TX, average of taxanes including paclitaxel and docetaxel; VA, average of *Vinca* alkaloids including vincristine, vindesine, vinblastine; D10, dolastatin 10; TZT, TZT-1027.

Table 4 Discriminatory genes of *Vinca* alkaloids (vindesine, vincristine, vinblastine)

GB	*Symbol*	*Description*	*Log ratio*			
			VA	*TX*	*D10*	*TZT*
Upregulated genes						
X14787	TSP1	Thrombospondin 1	0.319	−0.230	−0.106	−0.019
X07820	MMP10	Matrix metalloproteinase 10	0.273	−0.272	−0.297	−0.417
Downregulated genes						
D78367	KRT12	Keratin 12	−0.124	0.262	0.250	0.598
X03212	KRT7	Keratin 7	−0.168	0.412	0.004	0.290
X56134	VIM	Vimentin	−1.072	0.583	0.927	1.344

Abbreviations: GB, genebank accession number; VA, average of *Vinca* alkaloids including vincristine, vindesine, vinblastine; TX, average of taxanes including paclitaxel and docetaxel; D10, dolastatin 10; TZT, TZT-1027.

Table 5 Discriminatory genes between TZT-1027 and dolastatin 10

GB	*Symbol*	*Description*	*Log ratio*						
			TZT	*D10*	*VDS*	*VBL*	*VCR*	*TXL*	*TXT*
U59167	DESM	Desmin	1.74	−0.49	−0.28	0.06	−0.71	0.44	0.43
U34819	MAPK10	Mitogen-activated protein kinase 10	0.83	−0.69	−0.52	0.98	0.57	1.33	0.93
X14420	COL3A1	Collagen, type III, alpha 1	0.52	−0.92	0.56	−0.79	−0.38	−0.67	−0.66
X05610	COL4A2	Collagen, type IV, alpha 2	0.71	−0.53	0.82	0.32	0.10	−0.06	0.33
X16468	COL2A1	Collagen, type II, alpha 1	1.08	−0.01	0.99	−0.08	0.56	0.36	−0.07
U33635	PTK7	Tyrosine-protein kinase-like 7	0.62	−0.45	0.04	0.56	0.68	0.15	0.05

Abbreviations: GB, genebank accession number; TZT, TZT-1027; D10, dolastatin 10; VDS, vindesine; VBL, vinblastine; VCR, vincristine; TXL, paclitaxel; TXT, docetaxel.

Of the 588 genes that were surveyed, about half of all the genes were regulated similarly by the seven drugs. The probability of these similar expression profiles occurring by chance is almost zero ($P<1\times10^{-100}$). Furthermore, the functions of the clustered genes were associated with microtubule dynamics. The 118 genes that were upregulated were significantly associated with cell-cycle regulation, mitosis or apoptosis, whereas the 141 genes that were

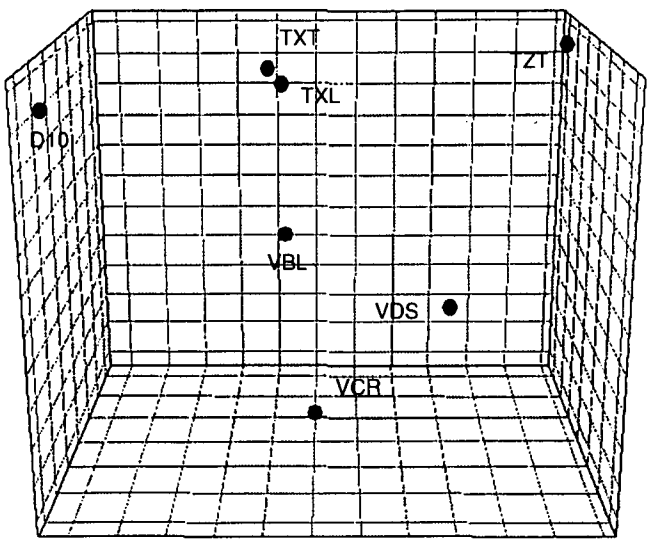

Figure 3 Spatial class separation of antimicrotubule agents using six genes from Table 5 that discriminated between TZT-1027 and dolastatin 10. TZT and D10 were distant from all the other antimicrotubule agents. TZT, TZT-1027; dolastatin 10, D10; VDS, vindesine; VCR, vincristine; VBL, vinblastine; TXL, paclitaxel; TXT, docetaxel.

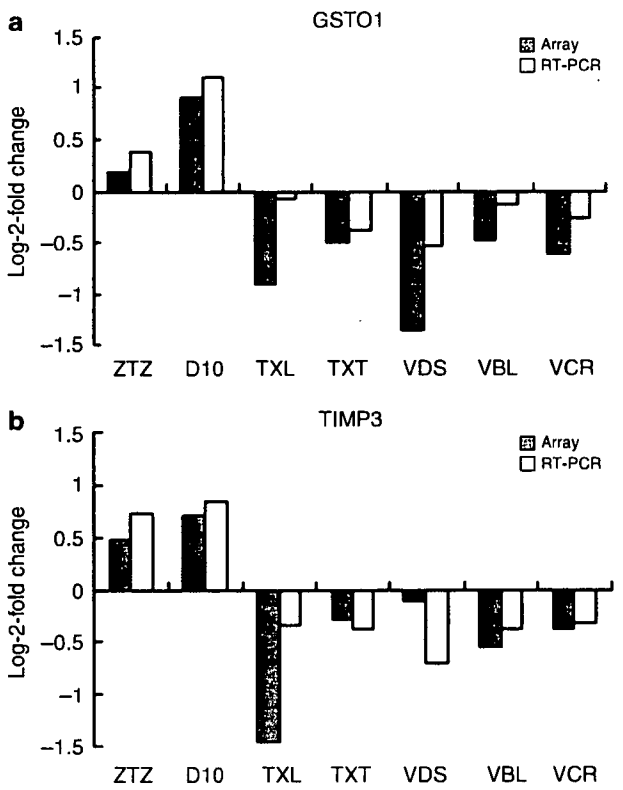

Figure 4 Gene expression of GSTO1 and TIMP3 in PC-14 cells treated with antimicrotubule agents. Validation of mRNA expression levels in PC-14 cells after 6 h of treatment with TZT-1027 (TZT), dolastatin 10 (D10), paclitaxel (TXL), docetaxel (TXT), vindesine (VDS), vinblastine (VBL) or vincristine (VCR). Relative mRNA amounts were normalized with respect to expression levels in untreated PC-14 cells (Log-2-fold change = 0).

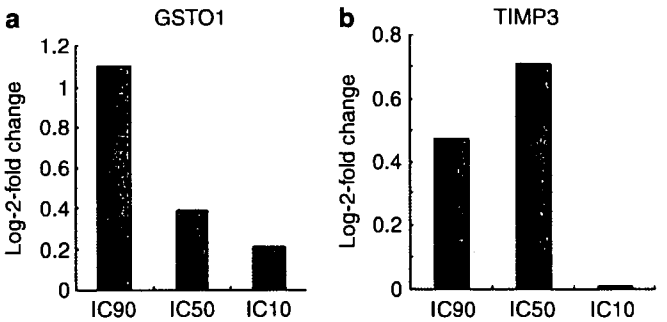

Figure 5 (**a**) Gene expression of GSTO1 in PC-14 cells treated with TZT-1027 at IC_{90}, IC_{50} or IC_{10}. (**b**) Gene expression of TIMP3 in PC-14 cells treated with TZT-1027 at IC_{90}, IC_{50} or IC_{10}. Validation of mRNA expression levels in PC-14 cells after 6 h of treatment with TZT-1027 (TZT) at IC_{90} (0.1 nM) or IC_{10} (0.005 nM).

downregulated were associated with cell communication and morphogenesis. Therefore, we concluded that the genomic response profiles represented the drug activities in PC-14 cells and investigated the discriminatory genes within each drug class to enable their further characterization.

By comparing the resulting gene profiles, each drug was categorized according to its drug class based on its effects on microtubule modulation (Figure 1). This finding suggested that genomic response was mostly affected by the drug-binding site on the microtubules. TXT shares the same tubulin-binding site as TXL, and this site is distinct from the *Vinca* alkaloids binding site.[25] Although TXL has a 1.9-fold higher affinity for the binding site and polymerizes tubulin at 2.1-fold lower concentrations than TXL,[26] TXL and TXT induced similar gene expression profiles, compared with those induced by the other antimicrotubule drugs. Among the three *Vinca* alkaloids (VBL, VDS and VCR), the expression profile of VDS differed from those of the other two (Figure 6). Natsume *et al.*[14] reported that all three *Vinca* alkaloids inhibited the polymerization of microtubules at a similar affinity. VBL and VCR are structurally very similar, whereas the structure of VDS differs from those of the other two.[27] This structural difference may be responsible for the different genomic responses. *Vinca* alkaloids and dolastatins are known to bind at so-called *Vinca*-binding domains in tubulin.[25] They share the same binding site and have similar affinities,[14,28] whereas additional binding sites have either high affinities (Kd: 1–2 μmol) or low affinities (Kd: 0.25–3 μmol).[24] Previous studies have also reported that dolastatins can also bind at different sites from those used by *Vinca* alkaloids[14,29] These additional binding sites might be responsible for the differences in genomic response induced by the dolastatins and *Vinca* alkaloids.

Interestingly, of the 31 discriminatory genes that were selected, six of them were intermediate filament (IF) genes like desmin, vimentin, desmocollin and keratin (Tables 2, 4, 5). In addition, four collagen genes and one Rho-regulator gene were also selected. These genes are all associated with cytoskeletal regulation by the Rho signaling pathway via

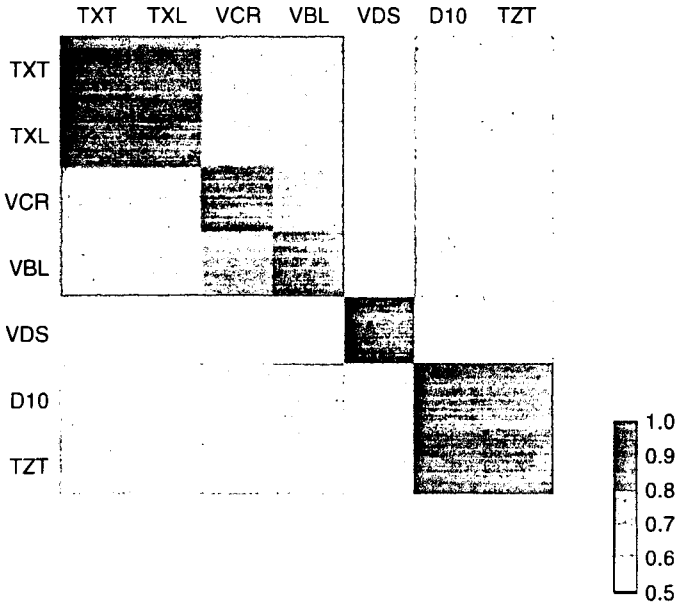

Figure 6 Heat map of correlations between drug profiles. Gene expression profiles containing data for 588 genes were compared after exposure to each drug to derive a matrix of Pearson correlation coefficients indicating the degree of overall similarity between any two drugs. A high-positive correlation is shown in red, and a low-positive correlation is shown in white. In this graph, TZT and D10 had the most similar expression profiles. TZT, TZT-1027; dolastatin 10, D10; VDS, vindesine; VCR, vincristine; VBL, vinblastine; TXL, paclitaxel; TXT, docetaxel.

microtubule dynamics.[30] Rho proteins also modulate the extracellular matrix either by regulating the levels of MMPs (matrix metalloproteinase) or their antagonists, TIMPs (tissue inhibitor of metalloproteinase).[31] These results suggested that the difference in the tubulin-drug binding site might regulate the difference in the signal transduction.

Of the genes that discriminated between dolastatins and the other drug class, the most significant genes were GSTO1 and TIMP3. GSTO1 (glutathione transferase omega 1) is a member of the glutathione *S*-transferase (GST) family of phase II enzymes that catalyze glutathione-dependent detoxification.[32] The role of GST has been evaluated in drug resistance. Schisselbauer *et al.* [33]reported that an elevated GST level in tumors was detected after the development of clinical drug resistance. Ban *et al.*[34] reported that adriamycin, cisplatin and etoposide increased tumor sensitivity by inhibiting GST expression in a colon cancer cell line, but TXL and VCR did not alter sensitivity. TIMP3 is a protein that binds to the extracellular matrix[35] and belongs to a family of endogenous MMP inhibitors. Members of the MMP family play important roles in angiogenesis.[36] Therefore, TIMP3 is regarded as a potent inhibitor of angiogenesis and tumor growth.[37] Qi *et al.*[38] reported that TIMP3 blocks the binding of VEGF (vascular endothelial growth factor) to the VEGF receptor-2, inhibiting downstream signaling and angiogenesis. TZT-1027 showed antitumor activity *in vivo* against a hypervascular advanced-stage tumor from a VEGF-transfectant lung cancer cell line, whereas VCR and TXT did not.[10] The upregulation of TIMP3 by TZT-1027 is one possible mechanism for the superior antivascular activity of this drug, compared to that of taxanes and *Vinca* alkaloids.

To analyze whether similar genomic responses occurred in lung cancer cell lines other than PC-14, RT-PCR for GSTO1 and TIMP3 was performed in another lung cancer cell line, SBC-3, treated with TZT-1027 at IC_{50}. GSTO1 and TIMP3 were downregulated in SBC-3 cells treated with dolastatins and upregulated in the cells treated with the other antimicrotubule agents, opposite to the profile seen for PC-14 cells (data not shown). This result suggested that these genes may have different genomic responses in other lung cancer cells.

This was a 'proof-of-principle study'. We demonstrated the various cellular responses to antimicrotubule agents at a gene expression level, even though the agents targeted the same molecules. We believe that this approach to characterizing drugs *in vitro* may be useful in clinical settings in that surrogate tissue, like peripheral blood mononuclear cells, can be used. The present findings obtained using our microarray analysis could greatly help us to understand the mode of action of TZT-1027 and other antimicrotubule agents. This capacity to identify therapeutic efficacy on the basis of gene expression signatures *in vitro* may be useful for drug discovery and drug target validation.

Materials and methods

Cell lines and cultures

A human non-small-cell-lung cancer cell line, PC-14, was provided by Professor Y Hayata, Tokyo Medical College. PC-14 was grown in RPMI-1640 medium (Nikken BioMedical Laboratory, Kyoto, Japan) supplemented with 10% fetal bovine serum, penicillin G and 100 μg/ml streptomycin solution and was maintained in a humidified 5% CO_2 atmosphere at 37°C.

Drugs and culture

TZT-1027 and D10 were provided by Teikoku Hormone Mfg. Co. Ltd (Kawasaki, Japan) and were dissolved in and diluted with 0.05 M lactate buffer (pH 4.5). Vindesine (VDS), vincristine (VCR), vinblastine (VBL), docetaxel (TXT) and paclitaxel (TXL) were obtained from Shionogi Co. (Osaka, Japan), Shionogi Pharmaceutical Co. (Osaka, Japan), Kyorin Pharmaceutical Co. Ltd (Tokyo, Japan), Chugai-Seiyaku Co, Ltd (Tokyo, Japan) and Bristol-Myers Japan (Tokyo, Japan), respectively. RPMI 1640 medium (Gibe-BRL) and fetal bovine serum were purchased from Nisus (Tokyo, Japan).

MTT assay

The inhibitory effect of the drugs on the PC-14 cell line was determined using a colorimetric assay (MTT assay) according to the method of Mosmann.[39] Briefly, 10^3 cells were harvested in 96-well microtiter plates (Becton Dickinson & Co.) in a volume of 180 μl and incubated for 24 h at 37°C in humidified air containing 5% CO_2. Each drug was added to

individual wells in a volume of 20 μl, and the cells were incubated for 72 h at 37°C in humidified air containing 5% CO_2. MTT reagents (MTT, Sigma) were then added to each well in a volume of 20 μl, and the cells were incubated for 4 h at 37°C in humidified air containing 5% CO_2. Finally, the growth inhibitory effect of each drug was assessed spectrophotometrically.

Drug treatment, RNA isolation and microarray hybridization

To obtain reference profiles representing the drug-induced genomic response, the PC-14 cells were grown on plastic culture dishes until they reached 80% confluency; they were then treated with TZT-1027, D10, VDS, VCR, VBL, TXL and TXT for 6 h at the IC_{50} concentration of each drug determined by MTT assay for 72 h. Cell pellets of the eight samples, including an untreated control, were collected by centrifugation, and the total RNA from each sample was isolated using a single-step guanidium thiocyanate procedure (ISOGEN; Nippon gene).[40] Single-channel labeling ^{32}P nylon membrane-based cDNA microarrays containing 588 genes were used (Atlas® Human Cancer cDNA Expression Array; BD Biosciences Clontech, Palo Alto, CA, USA). Protocols on array printing, labeling and hybridization are available at the BD Biosciences Clontech web site (http://www.bdbiosciences.com/clontech/atlas/index.shtml) The hybridization intensities on X-ray films (Gel Bond®, FMC Bio Products Rockland, ME, USA) were scanned and quantified using a BAS-2000II scanner and Array Gauge software (Fuji Film, Tokyo).

Microarray data analysis

The intensity values of each gene were log-2-transformed and median-normalized using Excel software. The changes in gene expression induced by drug exposure were calculated for each spot by dividing the intensity of the drug exposure samples by that of the untreated samples. The multidimensional scaling analysis, based on a principle component analysis, was performed using SIMCA-P software v10.5 (Umetrics, Sweden). Three-dimensional rendering of the gene profiles was graphed in a manner such that samples with similar expression profiles would lie closer to each other than those with dissimilar profiles. The heat map, which showed the correlation coefficient between each drug reference profile, was performed by *R* (http://cran.r-project.org/).

Functional analysis of identified genes

To analyze the functions of the clustered genes, a gene ontology analysis was performed using the EASE bioinformatics software package (http://apps1.niaid. nih.gov/david/upload.asp).[41,42] This software package was used to rank functional clusters by statistical over-representation of individual genes in specific categories relative to all genes in the same category on the array. The functional clusters used by EASE were derived from the classification systems of Gene Ontology (GO). The *P*-value to rank categories of genes by over-representation was calculated using Jackknife-Fisher exact probabilities. The threshold for selecting categories was a *P*-value of less than 0.01 and a minimum gene count of more than two. *P*-values in gene ontology are not equal to biological significance but are helpful in focusing on the processes most likely to be associated with the biological phenomena associated with aging. We also conducted further online database searches to refine many specific GO annotations.

Real-time RT-PCR

Real-time RT-PCR was performed using a Smart Cycler system (Takara) and a SYBR Green PCR kit. The reaction solution was assembled in a volume of 25 μl comprised of TaqMan™ Universal PCR Master Mix (Applied Biosystems, Foster City, CA, USA), forward and reverse primers (final concentration, 0.2 μmol/l each) and cDNA mixture ($\approx$2.5 ng) to produce PCR products specific for *GSTP1* and *TIMP3*. The primers and probes were purchased from Sigma-GenoSys (Tokyo, Japan). The conditions for real-time RT-PCR were preheating at 95°C for 10 min, followed by 40 cycles of shuttle heating at 95°C for 15 s and at 60°C for 20 s. A threshold was set in the linear part of the amplification curve, and the number of cycles needed to reach it was calculated for every gene. Relative mRNA levels were determined using the included standard curves for each individual gene and further normalized to the GAPDH mRNA level. Melting curves were used to establish the purity of the amplified band. The sequences of the primers used for RT-PCR were as follows: GSTO1 forward, 5′-AGG TTC TGC CCG TTT GCT GAG AGG and reverse, 5′-CAA GCT TTC TCA TAG GGG TCA TCC G; TIMP3 forward, 5′-TGC TGA CAG GTC GCG TCT ATG ATG G and reverse, 5′-GCG TAG TGT TTG GAC TGG TAG CCA G; GAPDH forward, 5′-TGA AGG TCG GAG TCA ACG GAT TTG GT and reverse, 5′-CAT GTG GGC CAT GAG GTC CAC CAC.

Acknowledgments

This study was supported in part by a Grant-in-Aid for Cancer Research and the 3rd Term Comprehensive 10-Year Strategy for Cancer Control from the Ministry of Health, Labour and Welfare, Tokyo, Japan. K Nishio and T Shimoyama designed the study. T Shimoyama and K Nishio prepared the manuscript. Y Koh and T Natsume undertook the study. T Shimoyama and T Hamano performed the statistical analysis. T Shimoyama is the recipient of a Research Resident Fellowship from the Foundation of Promotion of Cancer Research in Japan.

Duality of Interest

None declared.

References

1 Pettit G, Kamano Y, Herald C, Tuinman A, Boettner F, Kizu H *et al.* The isolation and structure of a remarkable marine animal antineoplastic constituent: dolastatin 10. *J Am Chem Soc* 1987; **109**: 6883–6885.
2 Saad ED, Kraut EH, Hoff PM, Moore Jr DF, Jones D, Pazdur R *et al.* Phase II study of dolastatin-10 as first-line treatment for advanced colorectal cancer. *Am J Clin Oncol* 2002; **25**: 451–453.

3 Vaishampayan U, Glode M, Du W, Kraft A, Hudes G, Wright J *et al.* Phase II study of dolastatin-10 in patients with hormone-refractory metastatic prostate adenocarcinoma. *Clin Cancer Res* 2000; **6**: 4205–4208.
4 Krug LM, Miller VA, Kalemkerian GP, Kraut MJ, Ng KK, Heelan RT *et al.* Phase II study of dolastatin-10 in patients with advanced non-small-cell lung cancer. *Ann Oncol* 2000; **11**: 227–228.
5 Margolin K, Longmate J, Synold TW, Gandara DR, Weber J, Gonzalez R *et al.* Dolastatin-10 in metastatic melanoma: a phase II and pharmokinetic trial of the California Cancer Consortium. *Invest New Drugs* 2001; **19**: 335–340.
6 Miyazaki K, Kobayashi M, Natsume T, Gondo M, Mikami T, Sakakibara K *et al.* Synthesis and antitumor activity of novel dolastatin 10 analogs. *Chem Pharm Bull (Tokyo)* 1995; **43**: 1706–1718.
7 Kobayashi M, Natsume T, Tamaoki S, Watanabe J, Asano H, Mikami T *et al.* Antitumor activity of TZT-1027, a novel dolastatin 10 derivative. *Jpn J Cancer Res* 1997; **88**: 316–327.
8 Chaplin DJ, Pettit GR, Parkins CS, Hill SA. Antivascular approaches to solid tumour therapy: evaluation of tubulin binding agents. *Br J Cancer Suppl* 1996; **27**: S86–S88.
9 Otani M, Natsume T, Watanabe JI, Kobayashi M, Murakoshi M, Mikami T *et al.* TZT-1027, an antimicrotubule agent, attacks tumor vasculature and induces tumor cell death. *Jpn J Cancer Res* 2000; **91**: 837–844.
10 Natsume T, Watanabe J, Koh Y, Fujio N, Ohe Y, Horiuchi T *et al.* Antitumor activity of TZT-1027 (Soblidotin) against vascular endothelial growth factor-secreting human lung cancer *in vivo*. *Cancer Sci* 2003; **94**: 826–833.
11 Niitani H, Hasegawa K. Phase I studies of TZT-1027, a novel inhibitor of tubulin polymerization. *Ann Oncol* 1998; **9**(Suppl 2): 360.
12 de Jonge MJ, van der Gaast A, Planting AS, van Doorn L, Lems A, Boot I *et al.* Phase I and pharmacokinetic study of the dolastatin 10 analogue TZT-1027, given on days 1 and 8 of a 3-week cycle in patients with advanced solid tumors. *Clin Cancer Res* 2005; **11**: 3806–3813.
13 Schoffski P, Thate B, Beutel G, Bolte O, Otto D, Hofmann M *et al.* Phase I and pharmacokinetic study of TZT-1027, a novel synthetic dolastatin 10 derivative, administered as a 1-hour intravenous infusion every 3 weeks in patients with advanced refractory cancer. *Ann Oncol* 2004; **15**: 671–679.
14 Natsume T, Watanabe J, Tamaoki S, Fujio N, Miyasaka K, Kobayashi M. Characterization of the interaction of TZT-1027, a potent antitumor agent, with tubulin. *Jpn J Cancer Res* 2000; **91**: 737–747.
15 Fujita F, Koike M, Fujita M, Sakamoto Y, Tsukagoshi S. Antitumor effects of TZT-1027, a novel dolastatin 10 derivative, on human tumor xenografts in nude mice. *Gan To Kagaku Ryoho* 2000; **27**: 451–458.
16 Watanabe J, Natsume T, Fujio N, Miyasaka K, Kobayashi M. Induction of apoptosis in human cancer cells by TZT-1027, an antimicrotubule agent. *Apoptosis* 2000; **5**: 345–353.
17 Natsume T, Kobayashi M, Fujimoto S. Association of p53 gene mutations with sensitivity to TZT-1027 in patients with clinical lung and renal carcinoma. *Cancer* 2001; **92**: 386–394.
18 Natsume T, Nakamura T, Koh Y, Kobayashi M, Saijo N, Nishio K. Gene expression profiling of exposure to TZT-1027, a novel microtubule-interfering agent, in non-small cell lung cancer PC-14 cells and astrocytes. *Invest New Drugs* 2001; **19**: 293–302.
19 DeRisi JL, Iyer VR, Brown PO. Exploring the metabolic and genetic control of gene expression on a genomic scale. *Science* 1997; **278**: 680–686.
20 Parsons AB, Brost RL, Ding H, Li Z, Zhang C, Sheikh B *et al.* Integration of chemical-genetic and genetic interaction data links bioactive compounds to cellular target pathways. *Nat Biotechnol* 2004; **22**: 62–69.
21 Baetz K, McHardy L, Gable K, Tarling T, Reberioux D, Bryan J *et al.* Yeast genome-wide drug-induced haploinsufficiency screen to determine drug mode of action. *Proc Natl Acad Sci USA* 2004; **101**: 4525–4530.
22 Kung C, Kenski DM, Dickerson SH, Howson RW, Kuyper LF, Madhani HD *et al.* Chemical genomic profiling to identify intracellular targets of a multiplex kinase inhibitor. *Proc Natl Acad Sci USA* 2005; **102**: 3587–3592.
23 Gunther EC, Stone DJ, Gerwien RW, Bento P, Heyes MP. Prediction of clinical drug efficacy by classification of drug-induced genomic expression profiles *in vitro*. *Proc Natl Acad Sci USA* 2003; **100**: 9608–9613.
24 DeVita VT, Hellman S, Rosenberg SA. *Cancer: Principles and Practice of Oncology*, 7th edn, Lippincott Williams & Wilkins (LWW): Philadelphia, 2004.
25 Jordan MA, Wilson L. Microtubules as a target for anticancer drugs. *Nat Rev Cancer* 2004; **4**: 253–265.
26 Diaz JF, Andreu JM. Assembly of purified GDP-tubulin into microtubules induced by taxol and taxotere: reversibility, ligand stoichiometry, and competition. *Biochemistry* 1993; **32**: 2747–2755.
27 Jordan A, Hadfield JA, Lawrence NJ, McGown AT. Tubulin as a target for anticancer drugs: agents which interact with the mitotic spindle. *Med Res Rev* 1998; **18**: 259–296.
28 Gupta S, Bhattacharyya B. Antimicrotubular drugs binding to *Vinca*domain of tubulin. *Mol Cell Biochem* 2003; **253**: 41–47.
29 Bai RL, Paull KD, Herald CL, Malspeis L, Pettit GR, Hamel E. Halichondrin B and homohalichondrin B, marine natural products binding in the *Vinca*domain of tubulin. Discovery of tubulin-based mechanism of action by analysis of differential cytotoxicity data. *J Biol Chem* 1991; **266**: 15882–15889.
30 Etienne-Manneville S, Hall A. Rho GTPases in cell biology. *Nature* 2002; **420**: 629–635.
31 Sahai E, Marshall CJ. RHO-GTPases and cancer. *Nat Rev Cancer* 2002; **2**: 133–142.
32 Board PG, Coggan M, Chelvanayagam G, Easteal S, Jermiin LS, Schulte GK *et al.* Identification, characterization, and crystal structure of the Omega class glutathione transferases. *J Biol Chem* 2000; **275**: 24798–24806.
33 Schisselbauer JC, Silber R, Papadopoulos E, Abrams K, LaCreta FP, Tew KD. Characterization of glutathione S-transferase expression in lymphocytes from chronic lymphocytic leukemia patients. *Cancer Res* 1990; **50**: 3562–3568.
34 Ban N, Takahashi Y, Takayama T, Kura T, Katahira T, Sakamaki S *et al.* Transfection of glutathione S-transferase (GST)-pi antisense complementary DNA increases the sensitivity of a colon cancer cell line to adriamycin, cisplatin, melphalan, and etoposide. *Cancer Res* 1996; **56**: 3577–3582.
35 Anand-Apte B, Bao L, Smith R, Iwata K, Olsen BR, Zetter B *et al.* A review of tissue inhibitor of metalloproteinases-3 (TIMP-3) and experimental analysis of its effect on primary tumor growth. *Biochem Cell Biol* 1996; **74**: 853–862.
36 Hiraoka N, Allen E, Apel IJ, Gyetko MR, Weiss SJ. Matrix metalloproteinases regulate neovascularization by acting as pericellular fibrinolysins. *Cell* 1998; **95**: 365–377.
37 Anand-Apte B, Pepper MS, Voest E, Montesano R, Olsen B, Murphy G *et al.* Inhibition of angiogenesis by tissue inhibitor of metalloproteinase-3. *Invest Ophthalmol Vis Sci* 1997; **38**: 817–823.
38 Qi JH, Ebrahem Q, Moore N, Murphy G, Claesson-Welsh L, Bond M *et al.* A novel function for tissue inhibitor of metalloproteinases-3 (TIMP3): inhibition of angiogenesis by blockage of VEGF binding to VEGF receptor-2. *Nat Med* 2003; **9**: 407–415.
39 Mosmann T. Rapid colorimetric assay for cellular growth and survival: application to proliferation and cytotoxicity assays. *J Immunol Methods* 1983; **65**: 55–63.
40 Chomczynski P, Sacchi N. Single-step method of RNA isolation by acid guanidinium thiocyanate-phenol-chloroform extraction. *Anal Biochem* 1987; **162**: 156–159.
41 Hosack DA, Dennis Jr G, Sherman BT, Lane HC, Lempicki RA. Identifying biological themes within lists of genes with EASE. *Genome Biol* 2003; **4**: R70.
42 Dennis Jr G, Sherman BT, Hosack DA, Yang J, Gao W, Lane HC *et al.* DAVID: database for annotation, visualization, and integrated discovery. *Genome Biol* 2003; **4**: P3.

Supplementary Information accompanies the paper on The Pharmacogenomics Journal website (http://www.nature.com/tpj).

Lung Cancer (2006) 53, 13–21

available at www.sciencedirect.com

SCIENCE DIRECT®

journal homepage: www.elsevier.com/locate/lungcan

LUNG CANCER

Effects of different combinations of gefitinib and irinotecan in lung cancer cell lines expressing wild or deletional EGFR

Tatsu Shimoyama[a,b], Fumiaki Koizumi[a], Hisao Fukumoto[a], Katsuyuki Kiura[b], Mitsune Tanimoto[b], Nagahiro Saijo[a], Kazuto Nishio[a,*]

[a] *Shien-Lab and Medical Oncology, National Cancer Center Hospital, Pharmacology Division, National Cancer Center Research Institute, Tsukiji 5-1-1, Chuo-ku, Tokyo 104-0045, Japan*

[b] *Department of Medicine II, Okayama University Medical School, 2-5-1 Shikata-cho, Okayama 700-8558, Japan*

Received 8 November 2005; accepted 1 March 2006

KEYWORDS
Gefitinib;
CPT-11;
SN-38;
EGFR;
Combination;
Lung cancer

Summary EGFR mutations are a major determinant of lung tumor response to gefitinib, an EGFR-specific tyrosine kinase inhibitor. Obtaining a response from lung tumors expressing wild-type EGFR is a major obstacle. The combination of gefitinib and cytotoxic drugs is one strategy against lung cancers expressing wild-type EGFR. The DNA topoisomerase inhibitor irinotecan sulfate (CPT-11) is active against lung cancer. We examined the sensitivity of lung cancers expressing wild- or mutant-type EGFR to the combination of gefitinib and CPT-11. The in vitro effect of gefitinib and SN-38 (the active metabolite of CPT-11) was examined in seven lung cancer cell lines using the dye formation assay with a combination index. When administered concurrently, gefitinib and SN-38 had a synergistic effect in five of the seven cell lines expressing wild-type EGFR, whereas the combination was antagonistic in PC-9 cells and a PC-9 subline resistant to gefitinib and expressing deletional mutant EGFR (PC-9/ZD). When administered sequentially, treatment with SN-38 followed by gefitinib had remarkable synergistic effects in the PC-9 and PC-9/ZD cells. In an in vivo tumor-bearing model, this combination had a schedule-dependent synergistic effect in the PC-9 and PC-9/ZD cells. An immunohistochemical analysis of the tumors in mice treated with CPT-11 and gefitinib demonstrated that the number of Ki-67 positive tumor cells induced by CPT-11 treatment was decreased when CPT-11 was administered in combination with gefitinib. In conclusion, the sequential combination of CPT-11 and gefitinib is considered to be active against lung cancer.

1. Introduction

Lung cancer is one of the leading causes of cancer-related death, despite the use of conventional chemotherapy regi-

* Corresponding author at: Tel.: +81 3 3542 2511; fax: +81 3 3547 5185.
E-mail address: knishio@gan2.res.ncc.go.jp (K. Nishio).

0169-5002/$ – see front matter © 2006 Elsevier Ireland Ltd. All rights reserved.
doi:10.1016/j.lungcan.2006.03.014

mens. The epidermal growth factor receptor (EGFR) is frequently expressed in non-small cell lung cancer (NSCLC) and is correlated with a poor prognosis. Gefitinib ('Iressa') is an orally active, selective EGFR-tyrosine kinase inhibitor that blocks signal transduction pathways. Its clinical efficacy has been show in refractory NCSLC patients, but the survival benefit of this agent remains unclear. EGFR mutations have been identified in NSCLC, and lung cancers carrying the EGFR mutation have been reported to be hyperresponsive to gefitinib [1,2]. Mutant EGFR is a major determinant of lung tumor response to gefitinib, but the hyperresponsiveness of tumors expressing mutant EGFR has been observed in a small population. Now, obtaining a clinical benefit in lung tumors expressing wild-ype EGFR is a major obstacle. The combination of gefitinib and cytotoxic drugs is one strategy against lung cancers expressing wild-type EGFR. The DNA topoisomerase I inhibitor irinotecan (CPT-11) is a key drug in the treatment of patients with lung cancer and has been shown to prolong survival. SN-38 is the active metabolite of CPT-11 in vitro. The objective of this study was to determine the potential therapeutic utility of gefitinib when combined with CPT-11 therapy to lung cancer cell according to the treatment schedule and EGFR status.

Acquired resistance to gefitinib is also of clinical interest. Recently, Kobayashi et al. [3] reported that an EGFR mutation was related to the development of acquired resistance to gefitinib. We have established subclone PC-9/ZD cells that are resistant to gefitinib [4]. Our results suggested that another mechanism of resistance was active in PC-9/ZD cells. The effect of the combination of gefitinib and SN-38 in these PC-9/ZD cells was also examined.

2. Materials and methods

2.1. Drugs and chemicals

Gefitinib (*N*-(3-chloro-4-fluorophenyl)-7-methoxy-6-[3-(morpholin-4-yl)propoxy]quinazolin-4-amine) was provided by AstraZeneca (Cheshire, UK). Gefitinib was dissolved in dimethyl sulfoxide (DMSO) for the in vitro study. CPT-11 and SN-38 were obtained from Yakult Honsha (Tokyo, Japan) and were dissolved in dimethyl sulfoxide (DMSO) for both of the in vitro studies.

2.2. Cells and cultures

Human NSCLC cell lines PC-9, PC-7, and PC-14 derived from untreated patients with pulmonary adenocarcinoma were provided by Professor Y. Hayata, Tokyo Medical College. A small cell lung cancer cell line, H69, was established at the National Cancer Institute (Bethesda, MD, USA). The gefitinib-resistant subline, PC-9/ZD, was established from intrinsic hypersensitive cell PC-9 [5] in our laboratory [4]. A small cell lung cancer cell line, SBC-3, and an adenocarcinoma cell line, A549, were obtained from the Japanese Cancer Research Resources Bank (Tokyo, Japan). All cell lines were maintained in RPMI1640 (Nikken Bio Med. Lab., Kyoto, Japan) supplemented with 10% heat-inactivated fetal calf serum, 100 μg/ml streptomycin, and 100 units/ml penicillin in an incubator at 37 °C and 100% humidity in 5% CO_2 and air, as described previously [6].

2.3. RT-PCR

Specific primers designed for EGFR CDS were used to detect the EGFR mRNA, as described elsewhere [1]. Sixteen first-strand cDNAs were synthesized from the cells' RNA using an RNA PCR Kit (TaKaRa Biomedicals, Ohtsu, Japan). After the reverse transcription of 1 μg of total RNA with Oligo(dT)-M4 adaptor primer, the whole mixture was used for PCR with two oligonucleotide primers (5′-AATGTGAGCAGAGGCAGGGA-3′ and 5′-GGCTTGGTTTGGAGCTTCTC-3). PCR was performed with an initial denaturation at 94 °C for 2 min and 25 cycles of amplification (denaturation at 94 °C for 30 s, annealing at 55 °C for 60 s, and extension at 72 °C for 105 s).

2.4. Western blot analysis

The cultured cells were washed twice with ice-cold phosphate buffered saline (PBS), lysate in EBC buffer (50 mM Tris–HCl, pH 8.0; 120 mM NaCl; 0.5% Nonidet P-40; 100 mM NaF; 200 mM Na orthovanadate; and 10 mg/ml each of leupeptin, aprotinin and phenylmethylsulfonyl fluoride). The lysate was cleared by centrifugation at 20,000 × *g* for 5 min, and the protein concentration of the supernatant was measured using a BCA protein assay (Pierce, Rockford, IL, USA). For immunoblotting, 20 μg samples of protein were electrophoretically separated on a 7.5% SDS-polyacrylamide gel and transferred to a polyvinylidene difluoride (PVDF) membrane (Millipore, Bedford, MA, USA). The membrane was then probed with rabbit polyclonal antibodies against EGFR, HER2/neu, Her3 and Her4 (Santa Cruz Biotech, Santa Cruz, CA, USA) and phospho-EGFR specific for Tyr 845, Tyr 1045, and Tyr 1068 (numbers 2231, 2235 and 2234; Cell Signaling, Beverly, MA, USA).

2.5. Growth-inhibition assay

We used the tetrazolium dye (3,(4,5-dimethyl-2-thiazolyl)-2,5-diphenyl-2H-tetrazolium bromide, MTT) assay to evaluate the cytotoxicity of various drug concentrations. After incubation for 72 h at 37 °C, 20 μl of MTT solution (5 mg/ml in PBS) was added to each well; the plates were then incubated for a further 4 h at 37 °C. After centrifuging the plates at 200 × *g* for 5 min, the medium was aspirated from each well and 180 μl of dimethylsulfoxide was added to each well to dissolve the formazan. Optical density was measured at 562 and 630 nm using a Delta Soft ELISA analysis program interfaced with a Bio-Tek Microplate Reader (EL-340; Bio-Metallics, Princeton, NJ, USA). Each experiment was performed in six replicate wells for each drug concentration and was independently performed three or four times. The IC_{50} value was defined as the concentration needed for a 50% reduction in the absorbance, as calculated based on the survival curves. Percent survival was calculated as follows:

$$\frac{\text{Mean absorbance of six replicate wells containing drugs} - \text{mean absorbance of six replicate background wells}}{\text{mean absorbance of six replicate drug-free wells} - \text{mean absorbance of six replicate background wells}} \times 100.$$

2.6. Combined effect of gefitinib and SN-38 in vitro

After 24 h of incubation, gefitinib and SN-38 were added to each cell line according to one of the two combination schedules. For the concurrent schedule, gefitinib and SN-38 were added concurrently and were then incubated under the same conditions for 72 h. For the sequential schedule, gefitinib or SN-38 were added sequentially and were then incubated under the same conditions for 72 h. The combined effect of gefitinib and SN-38 on lung cancer cell growth was evaluated using a combination index (CI) [7]. The CI was produced using CalcuSym software (Biosoft, NY, USA). For any given drug combination, the CI represents the degree of synergy, additivity, or antagonism. CI was expressed in terms of fraction-affected (F_a) values, which represents the percentage of cells killed or inhibited by the drug. Using mutually exclusive ($\alpha = 0$) or mutually non-exclusive ($\alpha = 1$) isobologram equations, the F_a/CI plots for each cell line were constructed by computer analysis of the data generated from the median effect analysis. The CI values were interpreted as follows: <1.0 = synergism; 1.0 = additive; >1.0 = antagonism.

2.7. In vivo growth-inhibition assay

Experiments were performed in accordance with the United Kingdom Coordinating Committee on Cancer Research Guidelines for the welfare of animals with experimental neoplasia (second edition). Fig. 2A shows the treatment schedule. For the in vivo experiments, the combined therapeutic effect of orally or intraperitoneally administered gefitinib and intravenously injected CPT-11 was evaluated according to a predetermined schedule. The dose of each drug was set based on the results of a preliminary experiment involving the administration of each drug alone. Ten days before administration, PC-9 and PC-9/ZD cells were injected subcutaneously into the backs of the mice. Six mice per group were injected with tumor cells. Tumor-bearing mice were given either gefitinib (40 mg/kg/day, p.o.) on days 2–6, CPT-11 (50 mg/kg/day, i.v.) on day 1, both, or a placebo (5%(w/v) glucose solution). Alternatively, tumor-bearing mice were given gefitinib on days 2–6 and CPT-1 on days 2. The diameters of the tumors were measured using calipers on days 1, 5, 8, 12, 15 and 20 to evaluate the effects of treatment, and tumor volume was determined using the following equation: tumor volume $ab^2/2$ (mm^3) (where a is the largest diameter of the tumor and b is the shortest diameter). Day 20 denotes the day on which the effects of the drugs were estimated, and day "0" denotes the first day of treatment. All mice were sacrificed on day 20 after their tumors had been measured.

2.8. Immunohistochemistry

The tumors were harvested from the mice at the time of sacrifice. For hematoxylin-eosin (HE) and anti-CD31 and Ki-67 staining, the resected tumors were fixed in zinc-buffered formalin (Shandon Lipshaw, Pittsburgh, PA) overnight at 4 °C. After paraffin embedding and sectioning at 6 μm, formalin-fixed sections were stained with Mayer's H&E (Richard Allen, Kalamazoo, MI, USA). For anti-Ki-67 and anti-CD31 immunohistochemistry, the slides were heated in a water bath at 95–99 °C in Target Retrieval Solution (DAKO, Carpinteria, CA, USA) for 20 min, followed by a 20-min cool-down period at room temperature. After heat retrieval, the sections were rinsed well in PBS and stained with rabbit antihuman Ki-67 antigen (DAKO N-series, ready to use) or rat antimouse CD-31 antibody (BD PharMingen, Tokyo, Japan) according to the manufacturer's instructions and then were lightly counterstained with Mayer's hematoxylin. The sections were finally stained with an in situ Death Detection POD Kit (Roche Diagnostic GmbH, Mannheim, Germany), according to the manufacturer's instructions.

TUNEL staining was performed using the Apoptosis Detection System, Fluorescein (Promega, Madison, WI, USA). Briefly, 6-μm cryostat sections were fixed in 4% paraformaldehyde for 10 min at room temperature and rinsed in PBS with 0.1% Triton X-100. The sections were then incubated in Equilibration Buffer for 5 min at room temperature followed by incubation in TUNEL Mix, prepared according to the manufacturer's instructions, for 1 h at 37 °C. After successive washes in PBS, the sections were coverslipped using an antifade reagent.

Microvessel density was determined by calculating the proportion of CD31-positive cells. The Proliferation Index was determined by Ki-67 immunostaining and calculating the population of Ki-67-positive cells in five fields at 200×. The Apoptosis Index, determined by TUNEL staining, was calculated from the population of TUNEL-positive cells in five fields at 200×. The apoptosis:proliferation ratio equals the apoptosis index/proliferation index × 100. At least 1000 tumor cell nuclei from the most evenly and distinctly labeled areas were examined in each examination.

At least 1000 cancer cells were counted and scored per slide. Both the percentage of specifically stained cells and the intensity of immunostaining were recorded. Blood vessels were detected with an anti-von Willebrand factor (vWF) antibody (Chemicon). Microvessel density was determined by calculating the proportion of vWF-positive cells.

3. Results

3.1. Expression of Her-receptors and cellular sensitivity to gefitinib or SN-38 in lung cancer cell lines

The expression levels of EGFR in seven lung cancer cell lines were examined using RT-PCR with a primer set for exon 20 in EGFR. PC-14, SBC-3, H69, PC-7, and A549 cells showed a 570-bp-long PCR amplified product exhibiting wild-type EGFR mRNA (data not shown). On the other hand, a smaller PCR product was also detected in the PC-9 and PC-9/ZD cells, and this band was confirmed to be an in-frame 15-base deletion of exon 20 (E746_A750del).

We examined the protein levels of EGFR, Her2, Her3, and Her4 in the lung cell lines using immunoblotting. The quantitative data obtained by densitometorical analysis is summarized in Table 1. The protein levels of EGFR, Her2, and Her3 in the PC-9 cells were one- to four-fold higher than those in the other cell lines (PC-7, H69, PC-14, A549, and SBC-3).

Table 1 Comparison of Her family protein levels and gefitinib- and SN-38-induced growth inhibition

Cell lines	Relative expression[a]				Growth inhibition[b], $IC_{50} \pm$ S.D.	
	EGFR	Her2	Her3	Her4	Gefitinib (μM)	SN-38 (nM)
PC-9	2.8[c]	3.2	3.7	ND	0.047 ± 0.061	8.09 ± 1.9
PC-9/ZD	1.6[c]	2.6	3.8	ND	7.7 ± 0.5	38.9 ± 7.0
PC-14	1.5	2.8	1.1	ND	17.1 ± 0.8	42.1 ± 2.6
SBC-3	2.4	2.6	1.0	ND	19.9 ± 5.4	1.07 ± 0.1
A549	2.3	2.3	1.4	ND	30.2 ± 2.2	293 ± 64.5
H69	1.3	1.3	2.0	ND	56.5 ± 3.2	27.2 ± 4.1
PC-7	1.0	1.0	1.2	ND	68.8 ± 14.8	20.5 ± 8.2

The IC_{50} value (μM) of each drug was measured by MTT assay, as described in Section 2. Each value is the mean ± S.D. of three or four independent experiments.

[a] Protein expression levels were analyzed by Western blotting.

[b] Drug concentration responsible for 50% growth inhibition in MTT assay at 72 h, calculated data for at least three dependent experiments.

[c] 15-base deletion EGFR, ND: not determined.

3.2. Cellular sensitivity of lung cancer cells to gefitinib and SN-38

The growth inhibitory effect of gefitinib and SN-38 on lung cancer cells was examined using an MTT assay. The IC_{50} values of gefitinib for the cell lines ranged from 46 nM (PC-9 cells) to 68 μM (PC-7 cells). The PC-9/ZD cells were ~200-fold resistant to gefitinib, compared with the parental PC-9 cells. Cellular sensitivity to gefitinib and the expression levels of EGFR and Her2 were negatively correlated with the IC_{50} values of gefitinib (Table 1). The IC_{50} values of SN-38 for these cell lines ranged from 1 nM (SBC-3) to 300 nM (A549). The range of sensitivity to gefitinib was wider than that to SN-38. No correlation in cellular sensitivity to gefitinib and SN-38 was seen.

3.3. In vitro combined effect of gefitinib and SN-38 on lung cancer cell lines

To evaluate the potential combined effect of gefitinib and SN-38, the combination index was determined using an MTT assay. The combined effects of gefitinib and SN-38 under the concurrent schedule are shown in Fig. 1. CI values of <1, >1, and 1 indicate a supra-additive effect (synergism), an antagonistic effect, and an additive effect, respectively. An additive to supra-additive growth-inhibitory effect was observed for all doses of gefitinib and SN-38 tested in cell lines expressing wild-type EGFR. On the other hand, a high CI index was observed in PC-9 cells and PC-9/ZD cells expressing mutant EGFR over a wide range of inhibition levels. These results suggest that gefitinib and SN-38 are synergistic in lung cancer cells expressing wild-type EGFR but not in cell lines expressing mutant EGFR in vitro.

3.4. Schedule-dependent synergy of gefitinib and SN-38 in lung cancer cells

Next, we examined the schedule dependency of the combined effects of gefitinib and SN-38 in the cell lines. The five cell lines expressing wild-type EGFR showed synergistic (PC-14, H69, and A549 cells) or additive effects (SBC-3 and PC-7 cells) for all three schedules: concurrent administration, SN-38 followed by gefitinib administration, and gefitinib followed by SN-38 administration (Fig. 1A). In the PC-9 cells, concurrent administration and gefitinib followed by SN-38 administration were antagonistic, but SN-38 followed by gefitinib administration was synergistic (Fig. 1B). In the PC-9/ZD cells, concurrent administration was antagonistic, but sequential administration was synergistic. These schedule-dependent combined effects were observed in the cells expressing mutant EGFR.

3.5. Combined effects of gefitinib and SN-38 in vivo

To estimate the schedule-dependent effects in vivo, nude mice bearing tumors were treated with gefitinib and CPT-11 according to sequential or concurrent schedules (Fig. 2A). Mice bearing PC-14 tumors were treated with gefitinib and CPT-11 according to sequential or concurrent schedules. CPT-11 (50 mg/kg) alone potentially reduced the tumor size, and the combination of gefitinib and CPT-11 was synergistic. In particular, the administration of CPT-11 followed by gefitinib cured the mice bearing PC-14 cells (Fig. 2B).

Mice bearing PC-9 or PC-9/ZD tumors were treated with gefitinib and CPT-11 according to sequential or concurrent schedules. Gefitinib (40 mg/kg) alone potentially reduced the PC-9 tumors, and CPT-11 (50 mg/kg) followed by gefitinib administration reduced the tumor size of PC-9 xenografts more dramatically (gefitinib alone: $P = 0.012$, sequential combination: $P = 0.005$) (Fig. 2B). On the other hand, the concurrent schedule produced an antagonistic effect. Body weight loss was not observed in any of the mice treated according to the above schedules (Fig. 2C). CPT-11 followed by gefitinib administration is a potentially beneficial schedule against PC-9 and PC-9/ZD cells expressing mutational EGFR. The results of these in vivo experiments were consistent with those of the in vitro studies.

To elucidate the synergistic mechanisms of CPT-11 and gefitinib in vivo, tumor samples of the PC-9 and PC-9/ZD

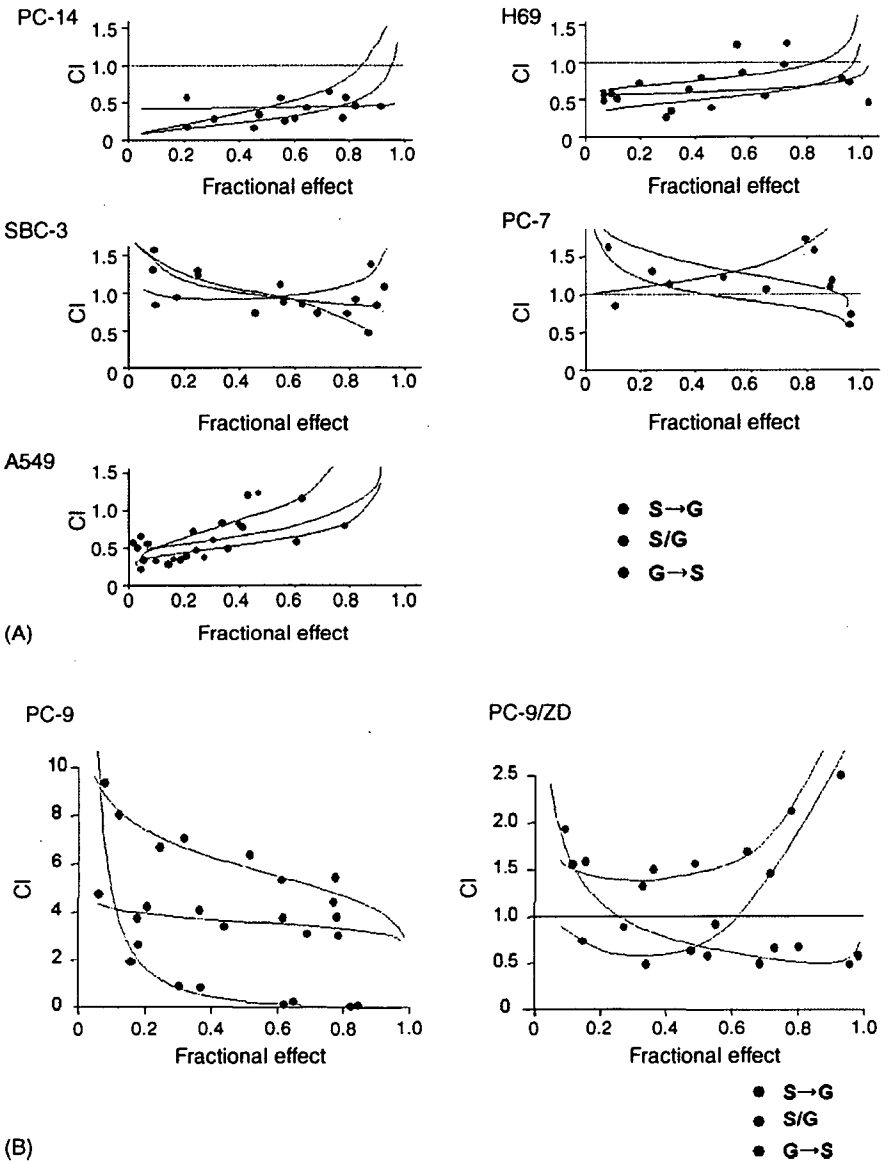

Fig. 1 Combination index (CI) plots of interactions between gefitinib and SN-38 in lung cancer cell lines. Each cell line was treated with gefitinib and SN-38, either alone or in combination at a fixed molar ratio. (A) (PC-14) gefitinib: SN-38 = 425:1; (SBC-3) 20000:1; (A549) 100:1; (H69) 2000:1; (PC-7) 3500:1. (B) (PC-9) gefitinib: SN-38 = 6:1; (PC-9ZD) 175:1. Treatment schedule: (1) SN-38 was applied first and gefitinib was applied 12 h later, followed by incubation in medium for 72 h (blue). (2) SN-8 and gefitinib were applied concurrently, followed by incubation in medium for 72 h (red). (3) Gefitinib was applied first and SN-38 was applied 12 h later, followed by incubation in medium for 72 h (green). S → G: sequential combination (SN-38 followed by gefitinib); C/G: concurrent combination; G → S: sequential combination (gefitinib followed by SN-38).

cells were stained with anti-Ki-67, anti-CD31 and the TUNEL assay (Fig. 3A and B). A reduction in tumor cell proliferation (Ki-67 staining), a reduction in tumor vasculature (CD31 staining), and an increase in tumor apoptosis (TUNEL staining) were observed in tumors treated with gefitinib alone or gefitinib and CPT-11. The administration of CPT-11 alone increased the number of Ki-67 positive tumor cells. In the PC-9 tumors, sequential treatment resulted in a 2.7-fold increase in tumor cell apoptosis and a 1.9-fold decrease in vessel staining, compared with the results obtained in tumors treated concurrently. The ratio of apoptosis:proliferation increased 1.7-fold in sequentially treated tumors compared with tumors treated with both drugs concurrently. Quantitative analysis of tumor cell proliferation and apoptosis showed a significant difference between the effects of the concurrent and sequential schedules ($P < 0.001$), but not between concurrent and gefitinib-alone ($P > 0.01$ for all comparisons, Fig. 3C). No significant difference in CD31-positive cells was observed between the control and gefitinib-alone treatments, suggesting that gefitinib exerts no remarkable anti-angiogenetic effects ($P > 0.01$, Fig. 3C). Similar findings were observed in PC-9/ZD tumors. These findings suggest that the antitumor activity of sequential treatment using gefitinib and CPT-11 is mediated by an increase in tumor cell apoptosis, compared with concurrent treatment.

4. Discussion

The EGFR-targeting drug gefitinib has been approved in many countries for the treatment of NSCLC patients who have previously received chemotherapy. Previous preclinical models have demonstrated the synergistic effects of gefitinib and platinums or taxanes [8,9]. However, no significant difference in survival was demonstrated in two randomized placebo-controlled phase II trials examining over 2000 previously untreated patients with NSCLC. In these trials, gefitinib was given in combination with paclitaxel and carboplatin or with gemcitabine and cisplatin [10,11]. Different administration schedules for gefitinib and cytotoxic agents may be necessary for select populations.

EGFR gene mutations have been demonstrated in NSCLC, and patients with lung cancers expressing mutant EGFR are strongly suspected to be hypersensitive to gefitinib alone. An in-frame short deletion in exon 19 of EGFR is strongly related to hyperresponsiveness to gefitinib and other tyrosine kinase inhibitors [12,13]. Cells expressing this deletional EGFR mutation are hypersenstivie to EGFR-targeted tyrosine kinase inhibitors [5]. On the other hand, the treat-

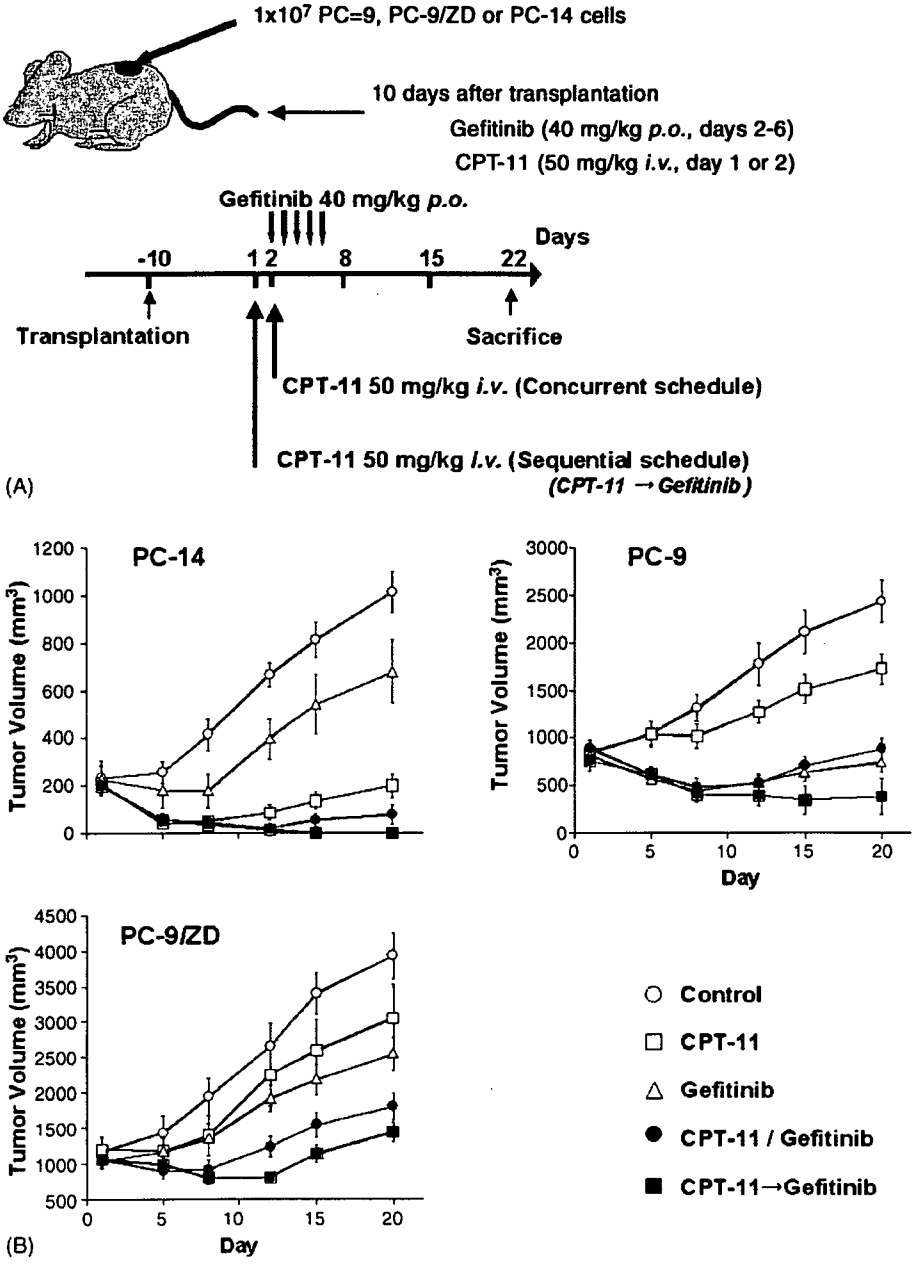

Fig. 2 Dose-dependent effects of combination therapy in PC9 and PC9/ZD cells in vivo. (A) Treatment schedule; (B) significant tumor growth-inhibition was observed in mice treated with the combination of gefitinib and CPT-11. Mice were allocated to five groups (6 mice/group) (○: 5% (w/v) glucose solution; □: CPT-11 50 mg/kg; △: gefitinib 40 mg/kg; ■: ZD1839 40 mg/kg + CPT-11 50 mg/kg concurrently; ●: CPT-11 50 mg/kg followed by ZD1839 40 mg/kg). (C) Treatment-related body weight loss in mice treated with gefitinib and/or SN-38. (○: 5% (w/v) glucose solution; □: CPT-11 50 mg/kg; △: ZD1839 40 mg/kg; ■: ZD1839 40 mg/kg + CPT-11 50 mg/kg concurrently; ●: CPT-11 50 mg/kg followed by ZD1839 40 mg/kg). Bars: ±S.D.

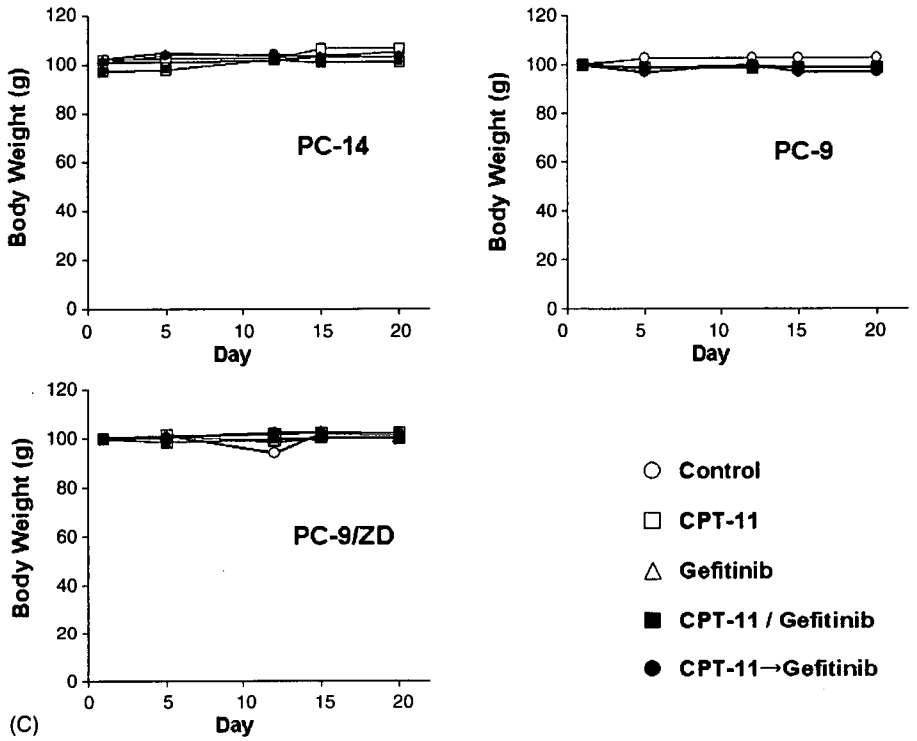

Fig. 2 (*Continued*).

ment of lung cancers expressing wild-type EGFR is a major obstacle. Combined therapies are still considered to be a major strategy against lung cancer expressing wild-type EGFR. Our previous preclinical study demonstrated that gefitinib and CPT-11 have synergistic effects in colorectal cancer cell lines [14]. Here, we reevaluated the combined effects of gefitinib and cytotoxic agents based on the status of EGFR mutations in lung cancer.

We demonstrated that gefitinib and SN-38, the active form of CPT-11, have synergistic or additive effects in lung cancer cells expressing wild-type EGFR. The combination of gefitinib and CPT-11 may be useful against lung cancers expressing wild-type EGFR. On the other hand, this combination had antagonistic effects in PC-9 cells expressing mutant EGFR, even though PC-9 cells are basically hypersensitive to gefitinib alone.

The concurrent administration of gefitinib and SN-38 also had an antagonistic effect in the PC-9/ZD cells. The PC-9/ZD cells developed an acquired resistance to gefitinib after exposure to gefitinib in vitro. New treatment strategies for patients who are refractory to gefitinib treatment are clinically needed. We demonstrated that the sequential administration of SN-38 (CPT-11) and gefitinib improved the combined effects in PC-9/ZD cells both in vitro and in vivo.

The above results led us to propose a combined gefitinib and CPT-11 treatment strategy based on the EGFR mutation status of lung cancers: (1) combined treatment according to any schedule for lung cancers expressing wild-type EGFR, (2) gefitinib treatment alone for lung cancers expressing mutant EGFR, and (3) the sequential administration of gefitinib and CPT-11 for patients who are refractory to gefitinib treatment. Based on the above preclinical evidence, we are preparing to begin a clinical phase II trial for combined gefitinib and CPT-11 treatment in Japan.

We previously demonstrated that CPT-11 and gefitinib have a synergistic effect against colorectal cancer [14]. EGFR mutations are rarely observed in colorectal cancer cells [15]. Therefore, the combined effects of these agents against colorectal cancers were consistent with those against the lung cancers expressing wild-type EGFR in this study.

Different combined effects were observed for the concurrent and sequential schedules in vitro and in vivo. While the mechanisms responsible for the combined effects remain unclear, cell cycle distributions might explain some of the differences. In cells treated according to the sequential gefitinib followed by SN-38 (CPT-11) treatment schedule, treatment with gefitinib resulted in an increase in the G0–G1 phase and a decrease in the S phase populations (data not shown). The decreased S phase population was not sensitive to CPT-11 [16]. Thus, the antagonistic effects of the sequential administration of gefitinib followed by CPT-11 (SN-38) could be explained by this mechanism. On the other hand, in cells treated according to the sequential SN-38 followed by gefitinib treatment schedule, SN-38 treatment induced an increase in the S phase population. If the S phase population is sensitive to gefitinib, this might explain the synergistic effects of this sequential schedule [17]. An increase in EGFR phosphorylation induced by CPT-11 is another previously reported possible mechanism responsible for this synergistic action [14].

In conclusion, we demonstrated the different effect on lung cancer cell expressing mutant EGFR according to the

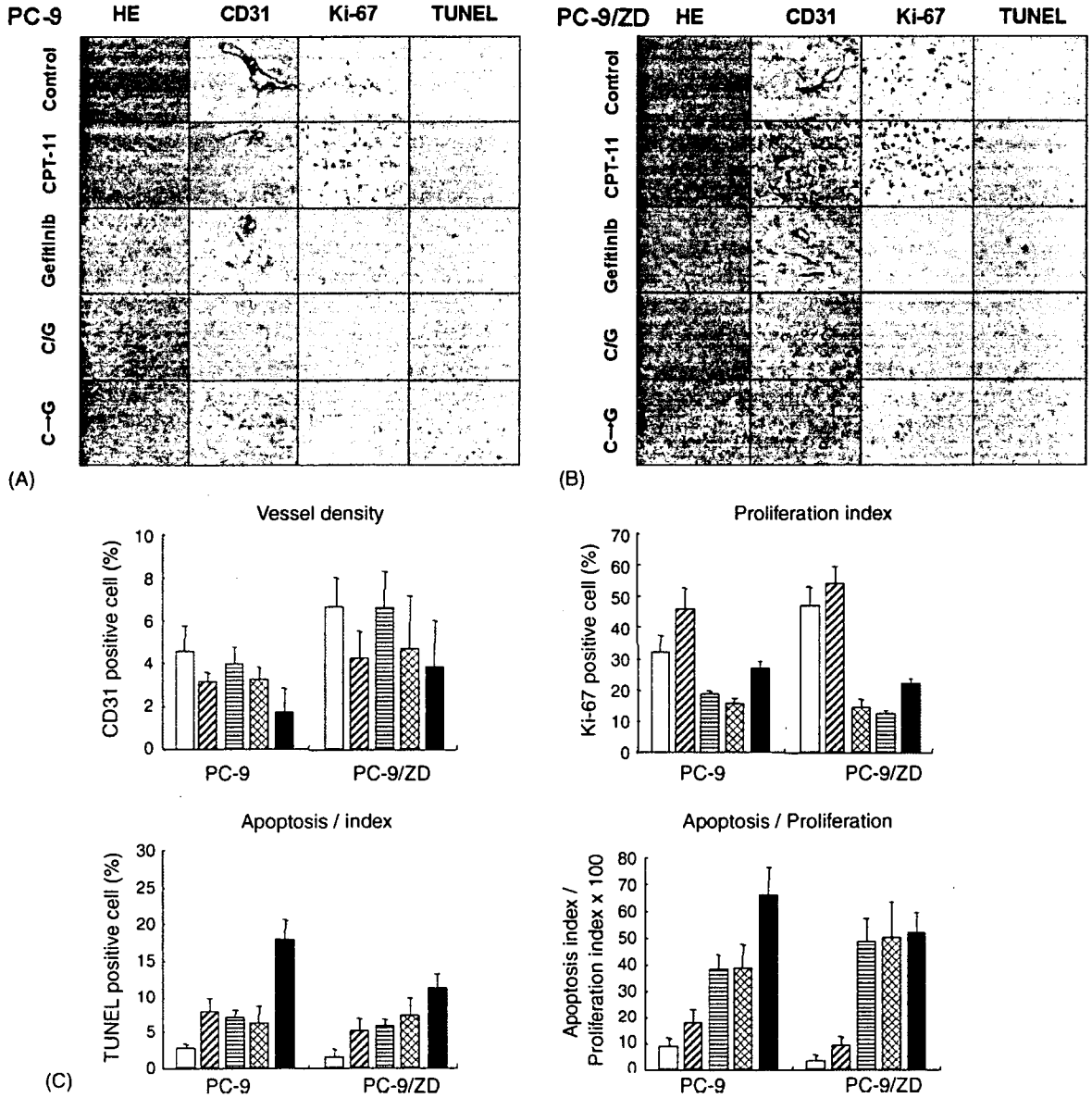

Fig. 3 (A) Historical examination of PC-9 tumor xenografts (day 22) stained with H&E, anti-CD31 vessel staining, TUNEL staining (magnification: 400×) and anti-Ki-67 nuclear antigen (magnification: 200×). The number of Ki-67-positive cells increased with the administration of CPT-11. The number of Ki-67-positive cells decreased with the gefitinib-alone and combination treatments. C/G: concurrent combination, C → G: sequential combination. (B) Historical examination of PC-9ZD tumor xenografts (day 22) stained with H&E, anti-CD31 vessel staining, TUNEL staining (magnification: 400×) and anti-Ki-67 nuclear antigen (magnification: 200×). The number of Ki-67-positive cells increased with the administration of CPT-11. The number of Ki-67-positive cells decreased with the gefitinib-alone and combination treatments. C → G: sequential combination; C/G: concurrent combination. (C) Quantitation of CD31 vessel staining, Ki-67 proliferation index, apoptosis index, and apoptosis: proliferation ratio. The columns represent the mean population of positive cells in five fields. Bars: ±S.D. Tumors from mice treated with vehicle (white), CPT-11 (diagonal hatched), Gefitinib (horizontal hatched), concurrent combination of CPT-11 plus Gefitinib (cross-hatched), or sequential combination of CPT-11 plus Gefitinib (cross-hatched).

combination schedule of gefitinib and CPT-11. The sequential combined treatment also active against lung cancer cell expressing wild-type EGFR.

Acknowledgements

This study was supported in part by a Grant-in-Aid for Cancer Research and the 3rd Term Comprehensive 10-Year Strategy for Cancer Control from the Ministry of Health, Labour and Welfare, Tokyo, Japan.

References

[1] Lynch TJ, Bell DW, Sordella R, Gurubhagavatula S, Okimoto RA, Brannigan BW, et al. Activating mutations in the epidermal growth factor receptor underlying responsiveness of non-small-

cell lung cancer to gefitinib. N Engl J Med 2004;350:2129–39.
[2] Paez JG, Janne PA, Lee JC, Tracy S, Greulich H, Gabriel S, et al. EGFR mutations in lung cancer: correlation with clinical response to gefitinib therapy. Science 2004;304:1497–500.
[3] Kobayashi S, Boggon TJ, Dayaram T, Janne PA, Kocher O, Meyerson M, et al. EGFR mutation and resistance of non-small-cell lung cancer to gefitinib. N Engl J Med 2005;352:786–92.
[4] Koizumi F, Shimoyama T, Taguchi F, Saijo N, Nishio K, Kanzawa F, et al. Establishment of a human non-small cell lung cancer cell line resistant to gefitinib Synergistic interaction between the EGFR tyrosine kinase inhibitor gefitinib ("Iressa") and the DNA topoisomerase I inhibitor CPT-11 (irinotecan) in human colorectal cancer cells. Int J Cancer 2005;116:36–44.
[5] Naruse I, Ohmori T, Ao Y, Fukumoto H, Kuroki T, Mori M, et al. Antitumor activity of the selective epidermal growth factor receptor-tyrosine kinase inhibitor (EGFR-TKI) Iressa (ZD1839) in an EGFR-expressing multidrug-resistant cell line in vitro and in vivo. Int J Cancer 2002;98:310–5.
[6] Kanzawa F, Akiyama Y, Saijo N, Nishio K. In vitro effects of combinations of cis-amminedichloro (2-methylpyridine) platinum(II) (ZD0473) with other novel anticancer drugs on the growth of SBC-3, a human small cell lung cancer cell line. Lung Cancer 2003;40:325–32.
[7] Chou TC, Talalay P. Quantitative analysis of dose-effect relationships: the combined effects of multiple drugs or enzyme inhibitors. Adv Enzyme Regul 1984;22:27–55.
[8] Ciardiello F, Caputo R, Bianco R, Damiano V, Pomatico G, De Placido S, et al. Antitumor effect and potentiation of cytotoxic drugs activity in human cancer cells by ZD-1839 (Iressa), an epidermal growth factor receptor-selective tyrosine kinase inhibitor. Clin Cancer Res 2000;6:2053–63.
[9] Sirotnak FM, Zakowski MF, Miller VA, Scher HI, Kris MG. Efficacy of cytotoxic agents against human tumor xenografts is markedly enhanced by coadministration of ZD1839 (Iressa), an inhibitor of EGFR tyrosine kinase. Clin Cancer Res 2000; 6:4885–92.
[10] Giaccone G, Herbst RS, Manegold C, Scagliotti G, Rosell R, Miller V, et al. Gefitinib in combination with gemcitabine and cisplatin in advanced non-small-cell lung cancer: a phase III trial—INTACT 1. J Clin Oncol 2004;22:777–84.
[11] Herbst RS, Giaccone G, Schiller JH, Natale RB, Miller V, Manegold C, et al. Gefitinib in combination with paclitaxel and carboplatin in advanced non-small-cell lung cancer: a phase III trial—INTACT 2. J Clin Oncol 2004;22:785–94.
[12] Taguchi F, Koh Y, Koizumi F, Tamura T, Saijo N, Nishio K. Anticancer effects of ZD6474, a VEGF receptor tyrosine kinase inhibitor, in gefitinib ("Iressa")-sensitive and resistant xenograft models. Cancer Sci 2004;95:984–9.
[13] Arao T, Fukumoto H, Takeda M, Tamura T, Saijo N, Nishio K. Small in-frame deletion in the epidermal growth factor receptor as a target for ZD6474. Cancer Res 2004;64:9101–4.
[14] Koizumi F, Kanzawa F, Ueda Y, Koh Y, Tsukiyama S, Taguchi F, et al. Synergistic interaction between the EGFR tyrosine kinase inhibitor gefitinib ("Iressa") and the DNA topoisomerase I inhibitor CPT-11 (irinotecan) in human colorectal cancer cells. Int J Cancer 2004;108:464–72.
[15] Barber TD, Vogelstein B, Kinzler KW, Velculescu VE. Somatic mutations of EGFR in colorectal cancers and glioblastomas. N Engl J Med 2004;351:2883.
[16] van Ark-Otte J, Kedde MA, van der Vijgh WJ, Dingemans AM, Jansen WJ, Pinedo HM, et al. Determinants of CPT-11 and SN-38 activities in human lung cancer cells. Br J Cancer 1998;77:2171–6.
[17] Park JK, Lee SH, Kang JH, Nishio K, Saijo N, Kuh HJ. Synergistic interaction between gefitinib (Iressa ZD1839) and paclitaxel against human gastric carcinoma cells. Anticancer Drugs 2004;15:809–18.

Acta Med Kinki Univ Vol. 31, No. 2, 57-62, 2006

Progress in the field of molecular biology and application of biotechnology to medical oncology

Kazuto Nishio and Tokuzo Arao

Department of Genome Biology, Kinki University School of Medicine, Osakasayama, Osaka 589-8511, Japan

Abstract

Recent progress in the field of molecular biology has been expected to contribute to progress in the field of clinical medicine. Personalized medicine could be achieved by pharmacogenomics. Prospective clinical studies using biomarkers are considered to be important. Investigators should plan the study design and carefully perform such studies.

Key words: Pharmacogenomics, DNA chip, biomarker, prediction

Introduction

Remarkable progress has been made in the field of molecular biology in the 20th century (Table 1). The entire human genome has been sequenced by the Human Genome Project. The 21st century is, therefore, called the "Post Genome" era and further advances in the clinical application of biotechnology are expected. Applied biotechnology is also useful for both diagnostic and therapeutic oncology. Here, we shall discuss the application of biotechnology to the field of medical oncology.

Table 1 Progress in the field of molecular biology during the 20th century

year	event
1890	Mendelism
1926	Genes on chromosome (Mogan)
1944	DNA as gene component (Fibree)
1953	Double helix of DNA (Watson & Crick)
1956	Replication enzyme of DNA (Komburg)
1973	Recombination technology (Cohen)
1985	PCR (Mullis)
1990	Start the Human Genome Project
1998	Deciphering the human genome proceed to multicellular organism
2001	Decoding of the human genome by Celera Genomics Co.

Tissue Banking

Genome biology is expected to be applied to drug development. Drug development, such as that of cytotoxic anticancer drugs and molecular target drugs in the field of oncology, is one of the most upcoming fields. The first and most important step of drug screening is target identification and the search for seeds. The next step is screening of the compounds, followed by preclinical and clinical studies. It is considered that genomic information effectively contributes to the target identification and its validation. To obtain data about the human genome, analysis of human materials is essential. This approach is called the "Reverse Translational Research". In the clinical setting, it is also called "Molecular Correlative Study". These approaches are adopted by government-supported projects both in Japan and abroad. Pharmaceutical companies also aggressively conduct a search for seeds. Mega-pharmas, in particular, have already established the banking system for human materials. Japan has also started a banking system, but it seems to be still immature and Japan still falls behind other countries. The process of collecting clinical samples is called "Tissue Banking" or simply "Banking".

Pharmacogenomics

The approach mentioned above is also applied in the clinical setting. One of the well-recognized approaches is "Personalized Medicine,"

that allows therapy to be customized to individuals by analyzing the individual's genome. Analysis of the genome is called "pharmacogenomics" when it is related to treatment with drugs. "Pharmacogenomics" is a word combining "genomics" and "pharmacology". Broadly, pharamcogenomics includes the analysis of gene products, such as RNA and proteins. The pharmacogenomic approach is considered to contribute to health and welfare. The US and other governments are encouraging this strategy. For example, the US government provides guidance to the industry on the process of Investigational New Drug (IND), New Drug Application (NDA), and Biologic Licence Application (BLA). In our country, the Ministry of Health, Welfare, and Labour has requested for genomic information obtained by the genomic testing in clinical studies for pharmaceutical companies.

Application of pharamcogenomics is expected in three major stages: discovery, preclinical, and clinical stages (Table 2). Three examples are provided as follows; i) research on gene-related diseases; ii) relationship between gene polymorphism and response to drug treatment; iii) genomic tests for the prediction of drug responses. Examples 2 and 3 are considered to be closely associated with cancer treatment and will directly contribute to the exclusion of patients with severe toxicities or to the selection of responders and non-responders to a particular treatment. The markers obtained by pharmacogenomics are called as "biomarkers".

Biomarkers for molecule-targeting drugs

We would like to consider biomarkers for target-based drugs. 1) Overexpression of the target molecule; this is often detected by immunohitochemical analysis. Amplification of target molecules is detected by FISH, CISH or PCR. Somatic mutations in tumor tissues are detected by direct sequencing or other PCR based assays. For the purification of tumor tissues, the microdissection technique is useful. There are biomarkers for conventional cytotoxic drugs. ERCC1 is an enzyme involved in DNA repair and its transcript levels have been reported to be related to the responses to platinum-containing regimens (e.g., cisplatin plus gemicitabine) in non-small cell lung cancer patients[1]. Thus, biomarkers could be determinants for predicting the sensitivity and responses of tumors to cytotoxic drugs.

As mentioned above, the EGFR somatic mutation in lung cancer is a hot topic. Strong correlation has been observed between EGFR somatic mutations and clinical responses to an EGFR-specific tyrosine kinase inhibitor, gefitinib. Thus, the EGFR mutation is a definite biomarker, and other somatic mutations of oncogenes in tumors have been also reported. These mutations could be used as new biomarkers to clarify subpopulations of patients that would respond to molecule-targeting drugs. Currently, trials for new molecule-targeting therapeutics are now underway for solid tumors. Treatment with angiogenesis inhibitors and antibodies are expected to improve the outcome of patients. New biomarkers need to be continually sought for this type of therapeutics.

Now, these molecular correlative studies are called as "Critical Path Research" in the field of drug development (Fig. 1).

Considering the background of aggressiveness of biomarker research, the average response to drugs is much lower than that of other diseases (Fig. 2).

The average response rate to anticancer drugs is 20-30%, which is inadequate. In order to improve the response rate to anticancer drugs, selection of subpopulations of patients that

Table 2 Three broad applications of pharmacogenomics

Discovery
Target identification
Mechanisms of Action
Target differentiation
Biomarker identification
Preclinical Toxicology
Toxicogenomics
In vivo mechanism of action
Biomarker identification
Clinical
In vivo mechanism of action
Biomarker development and validation

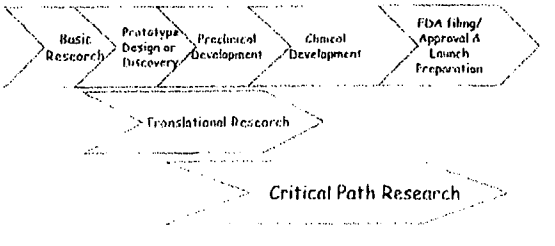

Fig. 1 Critical path. Significant benefit of bringing innovative products faster to the public

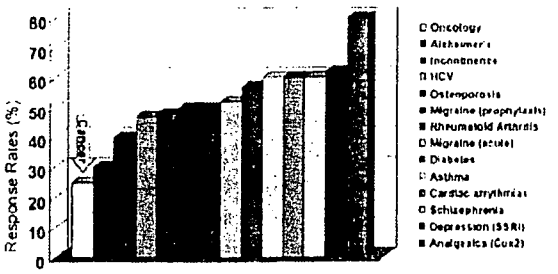

Fig. 2 The need for better predictive markers
(Paul Warning, Genentech, modified)

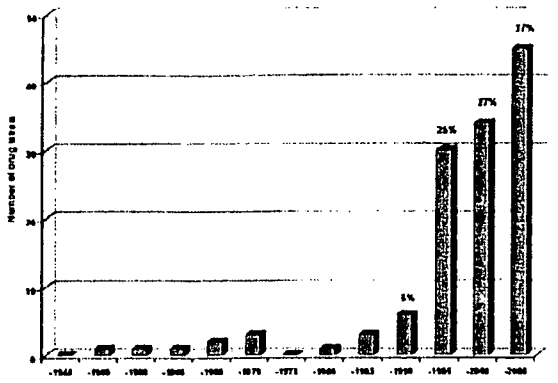

Fig. 3 Labels of approved drugs with pharmacogenomic information
(Frueh FW, CDER/FDA, modified)

would potentially show response is one strategy. At the same time, the labeling of drugs with pharmacogenomic data has been increasing recently (Fig. 3)

Government-related regulatory institutions in the US (Department of Health and Human Services, Food and Drug Administration, Center for Drug Evaluation and Research (CDER), Center for Biologic Evaluation and Research (CBER), Center for Devices and Radiological Health (CDRH)) developed a "Guideline for Industry," by which pharmaceutical companies are required to submit pharmacogenomic data. How should investigators assess/evaluate the data? Essentially, we should recognize three categories of pharmacogenomic information while selecting the treatment strategy: 1) test required, 2) test recommended, 3) information only.

Trastuzumab (Herceptin®) for breast cancer is a good example of the first; testing for anti-Her2 by FISH analysis (Herceptest®) is required for the administration of Trastuzumab. Although EGFR somatic mutation, EGFR immunohistochemistry, and FISH for EGFR are considered to be good biomarkers for predicting the response to EGFR-targeting drugs, they belong to the "Test only" category. It is not within the scope of this review to discuss why these differences exist. Anyway, applied pharmacogenomics is very important in the selection of appropriate subpopulations, and an increase in the number of "Test required" biomarkers is warranted.

Another point for discussion is that the pharmacogenomic approach has so far focused on the prediction or evaluation of adverse events. Single- nucleotide polymorphisms of metabolizing enzymes, such as p450 or UDP-glucuronoyltransferases (UGT)[2] are closely related to the toxicity profile of drugs. Therefore, tests for these genes are also included in the label of the drugs. The available evidence actually contributes to identify subpopulations of patients likely to show severe side effects. On the other hand, there is not much evidence, in terms of biomarkers, to distinguish accurately between responders and non-responders. It is important to consider the latter approach when considering personalized medicine.

Drug-diagnostic co-development

As mentioned before, the importance of pharmacogenomics has been discussed worldwide. Last year, the FDA proposed the new concept "drug-diagnostic co-development", although it is still in the draft stage and needs open discussion. What is the "co-development"? "Co-development" means: 1) Critical Path Research for biomarkers that would distinguish responders from non-responders in clinical studies; 2) research for avoiding severe toxicities; 3) clinical studies for POC (proof of concept) by monitoring pharmacodynamic markers. The endpoints of these approaches are to set the appropriate doses for each subpopulation or responders. Investigators should consider the study designs flexibly in these approaches. For example, randomized phase II studies and randomized discontinuation studies may be given more consideration. In addition, for the selection of biomarkers in Critical Path Research, more strict validation will be necessary, because the tests using the biomarkers will directly affect the treatment of each patient.

Problems in pharamcogenomics and future perspectives

Biomarker researches can be divided into two categories, "hypothesis-driven" and "hypothesis-free"; the former is to prove the power of preex-

isting biomarkers (predictability, reliability, specificity e.g.), whereas the latter is to select biomarkers without any hypothesis, by DNA microarray or proteomics. At the same time, validation of the selected biomarkers is necessary. Currently, the hypothesis-free approach seems to be the trend.

In general, biomarkers in the hypothesis-driven approach are relatively easy to understand, and are based on biological evidence. They can be expected to be more easily applied clinically. However, there is a limitation: only pre-existing biomarkers can be used. On the other hand, in the case of biomarkers in the hypothesis-free approach, it is difficult to understand underlying biological mechanisms and it is difficult to directly apply these markers clinically. However, novel biomarkers can be discovered by this approach.

When considering a new prospective study using microarray gene expression profiling, it is of importance to pay attention to some points, as follows. The investigators should recognize the role of quality assurance and perform the study accordingly. Regarding the data of DNA expression for Cancer Diagnostics, the guidelines proposed by the NCI-EORTC Working Group are helpful.[3] For the development of classifications based on the gene expression profile, the following points must be taken into consideration. 1) A common therapy is essential for identical populations. Are the results reasonable enough to establish a therapeutic policy? Will the new classification be generally used based on the cost-benefit balance, by comparing the selection of the therapies and the cost for mis-classified? These points should be discussed preliminarily during the process of designing of the study. For further evaluation, internal validation is necessary to prove the accuracy of the new classification in comparison with the pre-existing prognostic factors. The validation process includes 1) transfer to other platforms that are commonly used in clinical situations. (For example, will the classification identified by DNA chip analysis be valid for transfer to that by RT-PCR or immunohistochemical (ICH) examination), 2) confirmation of the reproducibility of the classification by the new platform (RT-PCR or ICH), and 3) independent validation in a prospective study. In addition, the investigators should recognize "multiplicity" of the comprehensive data sets, such as those of gene expression. Many researchers have reported classifiers to predict the prognosis of patients with cancers. For example, a 17- gene signature associated with metastasis was identified by a DNA chip analysis by Ramaswamy et al.[4] (Fig. 4)

Several researchers have attempted the same

Table 3 The 17 gene signature associated with metastasis

Gene	Gene name	GenBank ID
Upregulated in metastases		
SNRPF	Small nuclear ribonucleoprotein F	A1032612
EIF4EL3	Elongation initiation factor 4E-like 3	AF038957
HNRPAB	Heterogeneous nuclear ribonucleoprotein A/B	M65028
DHPS	Deoxyhypusine synthase	U79262
PTTG1	Securin	AA203476
COL1A1	Type I collagen, α1	Y15915
COL1A2	Type I collagen, α2	J03464
LMNB1	Lamin B1	L37747
Downregulated in metastases		
ACTG2	Actin, γ2	D00654
MYLK	Myosin light chain kinase	U48959
MYH11	Myosin, heavy chain 11	AF001548
CNN1	Calponin 1	D17408
HLA-DPB1	MHC Class II, DPβ1	M83664
RUNX1	Runt-related transcription factor 1	D43969
MT3	Metallothionein 3	S72043
NR4A1	Nuclear hormone receptor TR3	L13740
RBM5	RNA binding motif 5	AF091263